Structural Monitoring and Maintenance, *Vol. 6, No. 3 (2019) 237-254*
DOI: https:// doi.org/10.12989/smm.2019.6.3.237

Damage assessment of shear-type structures under varying mass effects

Ngoan T. Do, Qipei Mei and Mustafa Gül*

Department of Civil and Environmental Engineering, University of Alberta, 9211 116 St NW Edmonton, Alberta, Canada T6G 1H9

(Received June 7, 2019, Revised August 6, 2019, Accepted August 15, 2019)

Abstract. This paper presents an improved time series based damage detection approach with experimental verifications for detection, localization, and quantification of damage in shear-type structures under varying mass effects using output-only vibration data. The proposed method can be very effective for automated monitoring of buildings to develop proactive maintenance strategies. In this method, Auto-Regressive Moving Average models with eXogenous inputs (ARMAX) are built to represent the dynamic relationship of different sensor clusters. The damage features are extracted based on the relative difference of the ARMAX model coefficients to identify the existence, location and severity of damage of stiffness and mass separately. The results from a laboratory-scale shear type structure show that different damage scenarios are revealed successfully using the approach. At the end of this paper, the methodology limitations are also discussed, especially when simultaneous occurrence of mass and stiffness damage at multiple locations.

Keywords: structural health monitoring; damage detection; time series analysis; structural dynamics

1. Introduction

Over the past decades, structural health monitoring (SHM) systems have been increasingly implemented on various civil infrastructures, aerospace and mechanical systems due to its effectiveness in increasing the safety and reliability of structures (Balageas *et al*. 2006, Bas *et al*. 2017, Fan and Qiao 2011, He and Zhu 2011, Sony *et al*. 2019). Among SHM tasks, there is no doubt to say that the critical component is damage detection. In this context, damage detection is defined as a process that employs a variety of techniques to detect, locate, and quantify the damage caused by structural changes using vibration based monitoring data (Nguyen *et al*. 2018, Xi *et al*. 2018).

In damage detection process, local and global damage detection methods are two most general categories (Balageas *et al*. 2006). The process of detecting damage that happened locally at a specific time using modern techniques such as distributed fibre optic sensors, ultrasound is the priority of local methods, whereas global methods focus on condition assessment of the overall behaviour of structures mostly using dynamic response from which modal and physical parameters

*Corresponding author, Associate Professor, E-mail: mustafa.gul@ualberta.ca

http://www.techno-press.org/?journal=smm&subpage=7 ISSN: 2288-6605 (Print), 2288-6613 (Online)

such as natural frequencies, mode shapes, stiffness and damping coefficients are some of the useful properties estimated by numerous methodologies (Agarwal and Mitra 2014, Li and Wu 2007, Izuru and Nakamura 2000, Siebel *et al*. 2012, Soman *et al*. 2017, Takewaki and Nakamura 2005, Zhang and Johnson 2013a, b). However, there are a number of issues that need to be addressed before a vibration based damage detection framework can be routinely deployed in real-life applications. For instance, modal parameter based damage detection method is one of the most commonly applied global damage detection methods although the features may not be very sensitive to damage, especially under environmental and operational changes.

Among various SHM approaches, time series analysis based approaches have been widely used to analyse SHM data and to identify damage (Gül and Catbas 2009, Gül and Catbas 2011, Lu and Gao 2005, Omenzetter and Brownjohn 2006, Peter Carden and Brownjohn 2008, Roy *et al*. 2015, Shahidi *et al*. 2015). Auto-Regressive (AR) and Auto-Regressive Moving Average (ARMA) models are the early models employed for damage detection in SHM. These time series models show great potential in SHM applications since such statistical models can be effectively implemented in an automatic SHM system. A majority of recent applications of time series models has shown that the availability of current structural conditions is not required, which is more feasible for real-life applications. The following paragraphs summarise some remarkable studies that employ time series models for damage detection.

Loh *et al*. (2011) presented two methods for structural health monitoring by examining SHM data from the Fei-Tsui dam in Taiwan to define their trends and a threshold from which warning alarm will be activated if over-threshold occurs. Two methods, i.e. AR model and nonlinear Principal Component Analysis (PCA) using auto-associative neural network method (NPCA-AANN), were the proposed in the paper. The residual errors between the estimated trends and actual trends were computed, and subsequently the threshold was determined based on the training data. Piezoelectric active-sensing technique was applied to the recorded data from which time series models were employed to fit and build damage-sensitive features proposed by Figueiredo *et al*. (2012). Correlation analysis and PCA were then applied to the extracted features from the models to reduce their dimensions. Subsequently, Mahalanobis distance was used in a machine learning process to eliminate the environmental and operational effects. Results from the experimental composite plate showed that the damage was well identified. A study from Bao *et al*. (2013) proposed a combination of multiple techniques for damage detection where ARMA model was built to fit the acceleration data. Then, loading condition effects are reduced by introducing the partial auto-correlation function to optimize the AR parameters, which are in turn the damage indicators. Location of damage was identified based on the Mahalanobis distance of the estimated AR parameters for different damage cases.

It is worth noting that most studies were successful in identifying only the existence of damage, which is level 1 of damage detection according to the categorization proposed by Rytter (1993). This is apparently insufficient for real-life systems since location and severity of damage are equally important. Kuwabara *et al.* (2013) presented a method for system identification and damage detection of shear type high-rise buildings by using ARX models and then defined the limit of the identification function at zero frequency. The advantage of their method is that stiffness and damping of a story can be identified by simply using acceleration right above and below the story. However, only relatively large damage could be located and there was no information about the damage severity, and mass information of each floor is required as one of the inputs. Gül and Catbas (2008) presented their on-going research on a methodology where ARMAX model was utilized to build the statistical relationship among the response outputs at

different locations of structures based on the equation of motion. The numerical applications revealed very promising indications of the locations, and severity of different damage scenarios. In order to comprehensively describe the dynamic response using time series models and further improve the methodology, the authors advised that a more sophisticated derivations of the equation of motion should be conducted (Celik *et al*. 2018, Gül and Catbas 2009, Gül and Catbas 2011).

Operational effects such as additional mass coming from non-structural elements have an impact on system identification and damage detection since these effects can greatly alter the dynamic behaviour and damage indicators, which in turn reduce the effectiveness of the vibration based damage detection methodologies in use. For instance, Assi *et al*. (2016) showed that additional masses of non-structural components such as facades, glass panels and electrical equipment contribute to 21.7% reduction in first natural frequency of a six-storey reinforced concrete building. Mehdy Mehdi (2010) conducted modal tests on an office building floor from newly built to operational stage. It was shown that the experimental modal frequencies decreased by over 20% at the second stage (e.g., reducing from 3.25 Hz to 2.54 Hz) due to the additional mass of the non-structural elements. Effects of operational mass can be found in other studies conducted by Devin and Fanning (2012); Bighamian and Mirdamadi (2013).

The current paper can be considered as a follow-up study of the previous work by the authors (Mei and Gül 2015) where ARMAX models were used to fit acceleration response from multiple sensor clusters for localizing and quantifying the changes of mass and stiffness simultaneously with numerical applications only. In this paper, the authors continue to study the methodology on an experimental 4-story shear structure. It is shown in this paper that damage in shear-type structures (such as buildings) can be effectively detected, located and quantified even under varying mass effects using output-only vibration data. The proposed method can be very effective for automated monitoring of buildings to develop proactive maintenance strategies. The paper is organized as follows. Section 2 summarizes a brief introduction about time series models, and the main steps of the proposed method. Section 3 presents the experimental structure from which the proposed method is verified and validated via a series of damage scenarios. The effectiveness, and limitations of the method are also discussed.

2. Methodology

2.1 Time series model

The methodology used in this paper is based on ARMAX model, which can build the direct relationship between input and output variables. Full explanations of the model can be found in the literature (Box *et al*. 2016, Montgomery *et al*. 2008). The general form of the ARMAX model is in Eq. (1).

$$y(t)+a_1y(t-\Delta t)+\cdots+a_{n_a}y(t-n_a\Delta t)=b_1u(t-\Delta t)+\cdots+b_{n_b}u(t-n_b\Delta t) \\ +e(t)+d_1e(t-\Delta t)+\cdots+d_{n_c}e(t-n_c\Delta t) \tag{1}$$

where $y(t)$, $u(t)$ and $e(t)$ are output, input and error terms of the model, respectively; the parameters of the model are symbolized as $a_1,\dots,a_{n_a};b_1,\dots,b_{n_b};d_1,\dots,d_{n_c}$. A more general form of the model is shown in Eq. (2).

$$A(q)y(t) = B(q)u(t) + D(q)e(t) \tag{2}$$

where q is the back-shift operator. For example, if a time-dependant variable $x(t)$ is multiply by q^j, it will result in $x(t\text{-}j\Delta t)$. Therefore, $A(q)$, $B(q)$, and $D(q)$ can be expressed in the Eq. (3). The orders of the parameters of the model are denoted as n_a, n_b, and n_c. Different time series models can be created by adjusting the value of the model's orders. For example, an AR model with the order of n_c can be created by defining zero values for both n_b and n_c. The exogenous inputs in the model are expressed as the sequence $u(t)$.

$$\begin{aligned} A(q) &= 1 + a_1 q^{-1} + \cdots + a_{n_a} q^{-n_a} \\ B(q) &= b_1 q^{-1} + b_2 q^{-2} \cdots + b_{n_b} q^{-n_b} \\ D(q) &= 1 + d_1 q^{-1} + d_2 q^{-2} \cdots + d_{n_c} q^{-n_c} \end{aligned} \tag{3}$$

2.2 Building ARMAX models for different sensor clusters

The linear dynamic response of an N degree of freedom (DOF) system due to an excitation is described in the equation of motion given in Eq. (4), where $\boldsymbol{M}$, $\boldsymbol{C}$, and $\boldsymbol{K}$ are the mass, damping and stiffness properties in forms of matrices, respectively. The acceleration, velocity, and displacement vectors correspond to the terms $\ddot{\boldsymbol{x}}(\boldsymbol{t}), \dot{\boldsymbol{x}}(\boldsymbol{t}),$ and $\boldsymbol{x}(\boldsymbol{t})$ in Eq. (4). The excitation source is denoted by $\boldsymbol{f}$.

$$\boldsymbol{M}\ddot{\boldsymbol{x}}(t) + \boldsymbol{C}\dot{\boldsymbol{x}}(t) + \boldsymbol{K}\boldsymbol{x}(t) = \boldsymbol{f}(t) \tag{4}$$

Mathematical transformations of the equation of motion are introduced before fitting the ARMAX models with the dynamic response of the system. Firstly, the ith row of Eq. (4) is written separately in Eq. (5). After rearranging this equation, acceleration of the ith channel is described in terms of other components, which is shown in Eq. (6). It is assumed that mass of the system is lumped at each DOF. Therefore, the acceleration terms on the right side of Eq. (6) can be removed since any off-diagonal entries of the mass matrix are zeros. Also, preliminary analysis showed that the damping terms have very little effect on the balance of the equation, so they are ignored, and the simplified equation is shown in Eq. (7). As can be seen in Eq. (7), displacements are required, which is not easy to obtain in real-life application. Thus, it is worth trying to eliminate the displacement terms by taking the derivative of Eq. (7) twice which results in Eq. (8) where the fourth derivative of displacement, and accelerations are on the left and right sides of the equation, respectively. Finally, Eq. (9) is derived by employing the forward difference technique (Levy and Lessman 1961) twice on Eq. (8).

$$\left(m_{i1}\ddot{x}_1 + \cdots + m_{iN}\ddot{x}_N\right) + \left(c_{i1}\dot{x}_1 + \cdots + c_{iN}\dot{x}_N\right) + \left(k_{i1}x_1 + \cdots + k_{iN}x_N\right) = f_i \tag{5}$$

$$\begin{aligned} \ddot{x}_i = \frac{f_i}{m_{ii}} - \frac{m_{i1}\ddot{x}_1 + \cdots + m_{i,i-1}\ddot{x}_{i-1} + m_{i,i+1}\ddot{x}_{i+1} \cdots + m_{iN}\ddot{x}_N}{m_{ii}} \\ - \frac{c_{i1}\dot{x}_1 + c_{i2}\dot{x}_2 + \cdots + c_{iN}\dot{x}_N}{m_{ii}} - \frac{k_{i1}x_1 + k_{i2}x_2 + \cdots + k_{iN}x_N}{m_{ii}} \end{aligned} \tag{6}$$

$$\ddot{x}_i = \frac{f_i}{m_{ii}} - \frac{k_{i1}x_1 + k_{i2}x_2 + \cdots + k_{iN}x_N}{m_{ii}} \tag{7}$$

$$\dddot{x}_i = \frac{\ddot{f}_i}{m_{ii}} - \frac{k_{i1}\ddot{x}_1 + k_{i2}\ddot{x}_2 \cdots + k_{iN}\ddot{x}_N}{m_{ii}} \tag{8}$$

$$\frac{\frac{\ddot{x}_i(t+2\Delta t) - \ddot{x}_i(t+\Delta t)}{\Delta t} - \frac{\ddot{x}_i(t+\Delta t) - \ddot{x}_i(t)}{\Delta t}}{\Delta t} = \frac{\ddot{f}_i}{m_{ii}} - \frac{k_{i1}\ddot{x}_1(t) + k_{i2}\ddot{x}_2(t) + \cdots + k_{iN}\ddot{x}_N(t)}{m_{ii}} \tag{9}$$

It can be observed in Eq. (9) that $\ddot{x}_i(t)$ appears on both sides, which can cause trivial solutions to the parameters of ARMAX models. To overcome this problem, a new sequence $\ddot{y}_i(t)$ is defined as $y_i(t) = \ddot{x}_i(t+\Delta t) - \ddot{x}_i(t)$. The final form for the equation of motion of the i^{th} DOF is shown in Eq. (10), from which the change in the system's properties (mass and stiffness) can be treated as a function of change on the relation among the signals in different sensors.

$$\frac{y_i(t+\Delta t) - y_i(t)}{\Delta t^2} = \frac{\ddot{f}_i}{m_{ii}} - \frac{k_{i1}\ddot{x}_1(t) + k_{i2}\ddot{x}_2(t) + \cdots + k_{iN}\ddot{x}_N(t)}{m_{ii}} \tag{10}$$

Comparing Eq. (10) and Eq. (1), $y_i(t)$ and $\ddot{x}_i(t)$ are corresponding to output and input terms of the ARMAX model, respectively. The second derivative of excitation force can be assumed as white noise excitation represented by the error terms in the ARMAX models. It is decided that the order n_a and n_b of the ARMAX model can be assigned as 1 and 1 by aligning the input and output terms of the model and the corresponding entries in Eq. (10). After examining the residuals, n_c is chosen to be 15 to account for the errors caused by noise and transforming the equation of motion. The final ARMAX model represents the dynamic response of the i^{th} DOF can be approximately estimated as given in Eq. (11)

$$y_i(t+\Delta t) + a^i y_i(t) = b_1^i \ddot{x}_1(t) + b_2^i \ddot{x}_2(t) + \cdots + b_N^i \ddot{x}_N(t) + e(t) + d_1 e(t-\Delta t) + \cdots + d_{15} e(t-15\Delta t) \tag{11}$$

Similarly, it is straightforward to build N different ARMAX models for the remaining equations of motion of N DOF system. As mentioned above, the system has sparse stiffness and mass matrices meaning that the signal on a channel and its adjacent ones would interrelate closely. The ARMAX models are then simplified in a way that only the reference channel, and its neighbouring channels are present in the corresponding model. In this context, the sensor cluster technique proposed by Gül and Catbas (2011) has been employed such that an ARMAX model corresponds to a sensor cluster, and the output of the model is defined as the reference channel of the sensor cluster. It is expected that any changes in mass and stiffness would be revealed by examining changes in the ARMAX coefficients, which are the basics of building the damage-sensitive feature.

Once two sets of ARMAX models at the baseline and unknown case are successfully built, the location, and severity of damage in stiffness and mass can be revealed by choosing the appropriate damage feature (*DF*). In this study, the *DF* is defined as the relative difference of the *B(q)* coefficients at the unknown and baseline cases, which is shown in Eq. (12)

$$DF_{ij} = \frac{b^i_{j,baseline} - b^i_{j,damaged}}{b^i_{j,baseline}} \times 100\%$$
$$i \in sensor\ clusters, j \in adjacent\ sensors \tag{12}$$

In the next section, a description of a lab-scale shear-type structure and results for different damage scenarios are presented.

3. Experiments and results

3.1 Description of the structure

A lab-scale four-story shear structure was utilized for experimental verification of the methodology. As depicted in Fig. 1, the structure has four stories with height of 0.4 m for each story, and the floor area is 0.4 m×0.4 m. For the baseline case, sections L $31.75 \times 31.75 \times 4.76$ mm were used for columns, and they were connected to each other at each floor using bolts. In this way, damage in columns at different floors could be easily simulated by changing cross-sections or materials of columns. There was a steel plate attached at each floor using bolted connections to represent the extra lumped mass as a result of operational effects. As shown in Fig. 1, in order to prevent the structure from being exited in rotational mode, which is beyond the scope of the current study, the structure's base was rigidly clamped to the ground via an HSS beam.

The structure was triggered by ambient vibration, and monitored using only four accelerometers installed at one edge of each floor (Fig. 1). The accelerometers used herein are Integrated Electronics Piezoelectric (IEPE) uniaxial accelerometers from the PCB model 393A03 with a sensitivity of 1000 mV/g and a frequency range of 0.5 to 2000 Hz. The recorded dynamic response data were generated by randomly and simultaneously tapping the structure at the centre edges of any floors by impact hammer or fingertips, sample vibration data at each floor are shown in Fig. 2.

Table 1 Damage Patterns for the experimental structure

Damage Pattern (DP)	Descriptions
DP1	Replacing Two Thinner Columns between the First and Second Floors
DP2	Replacing Four Thinner Columns between the First and Second Floors
DP3	Replacing Two Thinner Columns between the 1st and 2nd floors; the 3rd and 4th floors
DP4	Removing One Plate at the Fourth Floor
DP5	Removing One Plate at the Fourth Floor + DP3

(a) Baseline case

(b) connection details

Fig. 1 The experimental structure

In the current study, five damage patterns listed in Table 1 are induced. For each damage scenario, 10 tests have been conducted and the damage features are shown as the average value and the standard deviation (in the parenthesis).

3.2 Damage Pattern 1 (DP1): Replacing two thinner columns between the first and second floors

The primary damage pattern introduces a stiffness reduction between the first and second floors. The computed *DFs* are shown in Table 2 where each row in the table is a sensor cluster, and each entry in the row represents the neighbouring sensors. For example, the first sensor cluster is placed in the first row, where acceleration at the 1st floor is the reference channel. Only the 2nd floor acceleration is the adjacent channel. Since accelerations at the 3rd and 4th floors are not directly

related to the 1st floor, so the last two columns in the first row are not applicable (N/A). To increase the statistical confidence, the results presented in percentage are the average of 10 trials and the values within the brackets are the standard deviation (also in percentage). It can be seen that the *DFs* around the 3rd and 4th floors are close to zero, showing that there is no damage occurred near these floors. However, top-left corner in the table shows some high values indicating that damage has affected the 1st and 2nd floors. Approximately, replacing two thinner columns ($I=1.827\times10^{-8}m^4$ would cause a decrease of $2\times[(I_d-I_b)]/[4\times I_b]\%=-14.28\%$ at K_{12}, $K_{21}$and $2\times[(I_d-I_b)]/[8\times I_b]\%=-7.14\%$ at K_{11}, K_{22} in the stiffness matrix of the structure. Table 2 shows that the values of DF_{12}, and DF_{21} are -9.06%; -8.58% respectively, whereas DF_{11} and DF_{22} show a reduction of 4.35% and 5.01%. In fact, the damage at the 1st floor linearly affects the structural stiffness at K_{12}, K_{21}, K_{11} and K_{22}. Therefore, the existence, location and severity of damage have been successfully detected. However, The *DFs* values are smaller than expected. One possible reason is that the overall stiffness of the structure is also affected by other components, e.g., connections, floor stiffness, etc. The standard deviations of the *DFs* in the parentheses demonstrate that the results are stable since most standard deviations are very small even though some DFs have greater standard deviations. However, these slightly greater standard deviations are still acceptable considering the noise from experimental data.

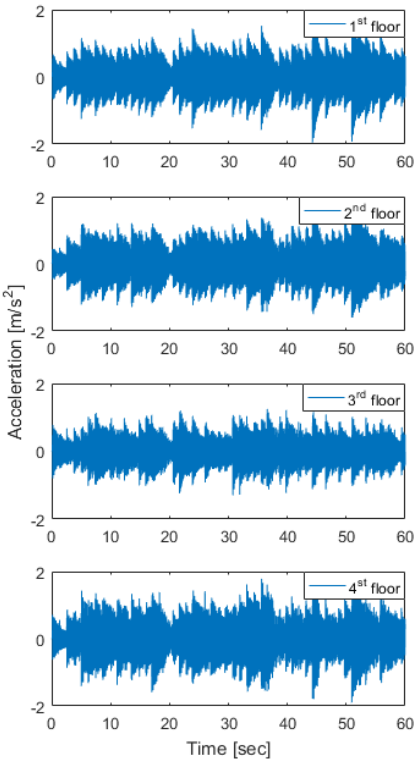

Fig. 2 Sample acceleration at four floors

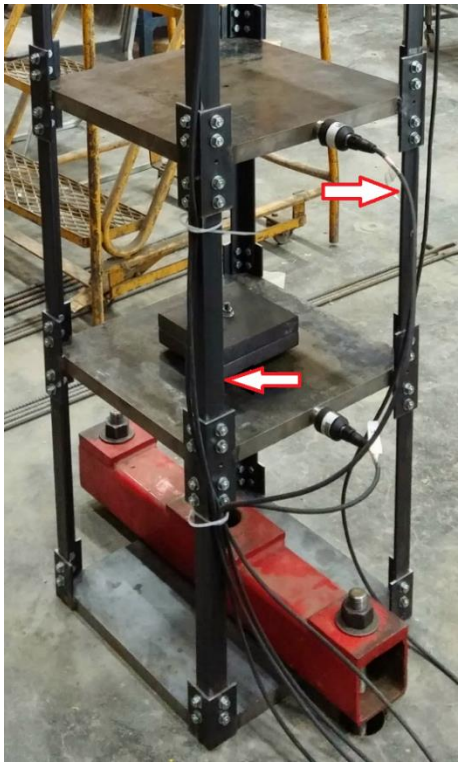

Fig. 3 Damage Pattern 1: Replacing two thinner columns between the first and second floors

Table 2 *DFs* in percentage for Damage Pattern 1 (Average and Standard Deviation in the parenthesis)

DOF	1st	2nd	3rd	4th
1st	-4.35 (0.54)	-9.06 (0.93)	N/A	N/A
2nd	-8.58 (1.23)	-5.01 (1.11)	-2.89 (2.28)	N/A
3rd	N/A	0.35 (1.65)	1.85 (0.99)	-0.18 (1.24)
4th	N/A	N/A	-0.38 (2.42)	1.15 (1.6)

3.3 Damage Pattern 2 (DP2): Replacing four thinner columns between the first and second floors

In order to further confirm that the methodology is able to reveal the severity of damage, all four columns between the first and second floors were replaced with thinner ones in this damage pattern, which is twice more severe (more stiffness reduction) than it was in Damage Pattern 1. It is observed from Table 3 that the *DFs* follow the same pattern as those in Table 2 since the damage occurred at the same location and only affected the first and second floors. DF_{11}, DF_{12}, DF_{21}, DF_{22} are about twice the corresponding *DFs* in DP1 as expected since using four thinner columns would result in twice stiffness reduction compared with two thinner columns in DP1.

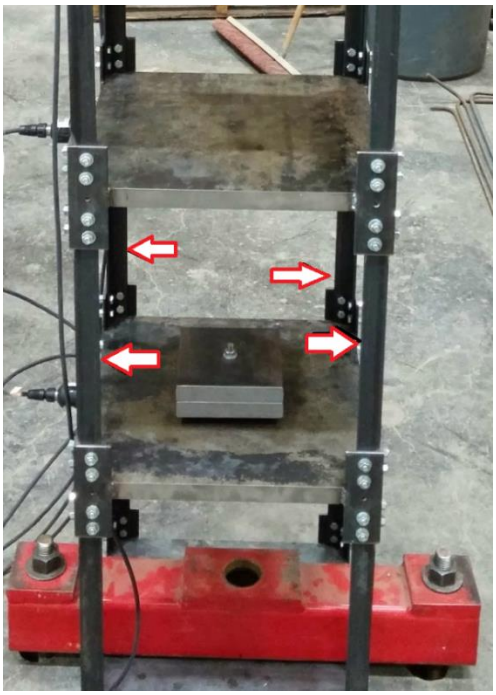

Fig. 4 Damage Pattern 2: Replacing four thinner columns between the first and second floors

Table 3 *DFs* in percentage for Damage Pattern 2 (Average and Standard Deviation in the parenthesis)

DOF	1st	2nd	3rd	4th
1st	-8.15 (1.08)	-18.00 (0.79)	N/A	N/A
2nd	-18.00 (1.44)	-10.38 (1.97)	-1.07 (3.39)	N/A
3rd	N/A	-0.29 (1.67)	0.35 (1.63)	-1.54 (0.97)
4th	N/A	N/A	-1.96 (2.04)	-0.57 (2.59)

3.4 Damage Pattern 3 (DP3): Replacing two thinner columns between the first and second floors; the third and fourth floors

Multiple damages caused by stiffness reduction were introduced in this case, where two thinner columns were used to replace the ones between the first and second floors and between the third and fourth floors. This damage case is similar to DP1 but at two locations simultaneously. Thus, it is expected that the *DFs* related to these floors would yield noticeable changes. It can be seen that the values at the left-top corner of Table 4 are almost the same as the corresponding *DFs* in Table 2, indicating that the location and severity of damage between the first and second floors are revealed successfully. In addition, the DFs between the third and fourth floors show how the stiffness in these floors changes due to the replacement of two columns. In terms of magnitudes,

the values of DF_{33} and DF_{44} are -3.68% and -9.41% implying how much the total stiffness on the third and fourth floors reduced due to the change of columns' cross-section. Furthermore, this damage creates approximately 7% stiffness reduction between the third and fourth floors.

Fig. 5 Damage Pattern 3: Replacing two thinner columns between the first and second floors; the third and fourth floors

Table 4 *DFs* in percentage for Damage Pattern 3 (Average and Standard Deviation in the parenthesis)

DOF	1st	2nd	3rd	4th
1st	-4.86 (0.19)	-9.74 (0.33)	N/A	N/A
2nd	-8.80 (1.71)	-5.99 (1.19)	-0.16 (3.36)	N/A
3rd	N/A	-0.52 (0.96)	-3.68 (0.58)	-6.00 (0.77)
4th	N/A	N/A	-7.48 (1.33)	-9.41 (0.82)

3.5 Damage Pattern 4 (DP4): Removing one plate at the fourth floor

The above sections demonstrate the effectiveness of the method in evaluating stiffness reduction. In this section, the plate mounted at the fourth floor was removed to simulate a reduction of mass. As calculated approximately, the percentage of mass reduction over the total weight of the fourth floor (40 kg) would be 11.3%. As explained in the methodology, the *DFs* represent both mass and stiffness information where the mass term is in the denominator, which means a reduction of 11% in mass would result in an increase of [1/(1-0.11)-1]%=12.4% in *DFs* in the entire corresponding sensor cluster or the corresponding row in the *DF* table. As shown in Table 5, the removal of the plate leads to an increase in all *DFs* of the fourth sensor cluster, i.e., DF_{43}, and DF_{44} (between 12 to 14%). The change at all entries in the fourth row is due to the 11% reduction in mass at this floor. This asymmetric phenomenon in the table is characterized as the main difference between changes in mass and stiffness whose change is approximately symmetrical. It is noted that there is a small change at DF_{23}, which is an error since this change is not consistent with the change in DF_{32} in the *DF* table. It could be caused by the noise while the experiment was being conducted.

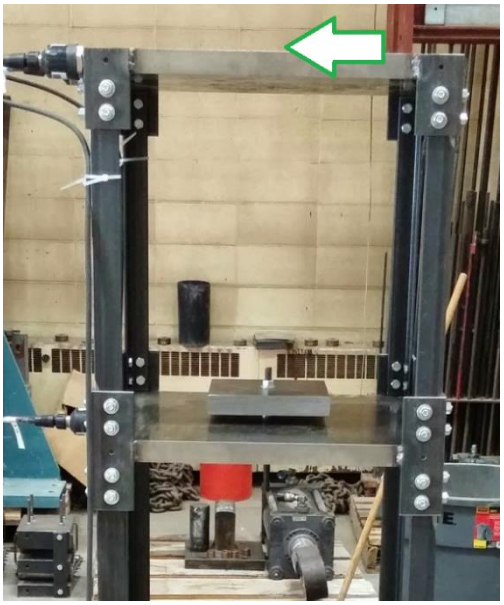

Fig. 6 Damage Pattern 4: Removing one plate at the fourth floor

Table 5 *DFs* in percentage for Damage Pattern 4 (Average and Standard Deviation in the parenthesis)

DOF	1st	2nd	3rd	4th
1st	-0.08 (0.37)	0.01 (0.69)	N/A	N/A
2nd	-1.01 (1.35)	-1.31 (1.02)	-3.55 (2.47)	N/A
3rd	N/A	-1.21 (1.45)	0.1 (0.74)	-0.19 (1.04)
4th	N/A	N/A	12.17 (1.39)	14.08 (0.61)

3.6 Damage Pattern 5 (DP5): Removing one plate at the fourth floor + DP3

Damage Pattern 5 introduces a damage caused by simultaneous occurrence of mass and stiffness changes at multiple locations. As can be seen in Table 6, the *DFs* between the first and second floors are close to the corresponding values in Table 2, which identifies the stiffness reduction between the first and second floors. In terms of the *DFs* between the third and fourth floors, DF_{33} and DF_{34} in the third row follow the same pattern as those from Table 4, which reveals the reduction in stiffness between the third and fourth floors. In the last row, two characteristics can be inferred due to the combination of simultaneous changes of stiffness and mass. DF_{33} and DF_{34} are caused by stiffness change only, whereas the results of DF_{43} and DF_{44} are due to the superposition of the two kinds of changes.

Fig. 7 Damage Pattern 5: Removing one plate at the fourth floor +DP3

Table 6 *DFs* in percentage for Damage Pattern 5 (Average and Standard Deviation in the parenthesis)

Ref. DOF	1st	2nd	3rd	4th
1st	-4.76 (0.13)	-9.36 (0.36)	N/A	N/A
2nd	-8.79 (1.19)	-5.65 (0.78)	-2.73 (2.25)	N/A
3rd	N/A	-0.08 (0.83)	-3.81 (0.66)	-6.76 (0.75)
4th	N/A	N/A	4.85 (1.52)	4.86 (0.27)

Therefore, it is concluded that there is a stiffness reduction between the third and fourth floors at around 7% when looking at the third row. Subsequently, the mass change can be evaluated based on the first conclusion and interpreting the last row. The total of 4.85% increase in the last row comes from the combination 7% stiffness reduction at K_{44}, and 11% mass reduction at m_4. As explained in the Eq. (10), where the mass term appears in the denominator, and thus the above stiffness and mass reduction would result in [(1-0.07)/(1-0.11)-1]=4.49% increase in DF_{43}, and DF_{44}, which is close to 4.85%. Overall, the first step is to interpret the *DFs* table is to analyse the stiffness reduction based on symmetric changes of the *DFs* in each sensor cluster (each row of the *DF* table), then evaluate mass change based on the asymmetric changes of the *DFs* from which the stiffness change can be revealed accordingly in each cluster.

3.7 Damage Pattern 6 (DP6): Removing one plate at the third floor + DP5

In this case, one more plate has been removed at the third floor along with the DP5, resulting in a more complicated damage scenario with both mass and stiffness changes. As observed in Table 7, the stiffness reduction between the first and second floors can be revealed since *DFs* representing these floors show the similar pattern as those in DP3. Regarding the third row and fourth rows in the table, asymmetric changes in DF_{34} and DF_{43} show that there must be a mass change related to these floors. Also, the changes in rows are inconsistent, which shows that there should be a stiffness reduction between the third and fourth floors. As it is described here, a detailed analysis of the damage feature table is needed to uncouple the damage and mass changes for very complicated scenarios. Firstly, the inequality between DF_{32} and DF_{23} indicates there was a mass reduction at the third floor (which is approximately 12% mass reduction as DF_{32} is 14.4%).

Table 7 *DFs* in percentage for Damage Pattern 6 (Average and Standard Deviation in the parenthesis)

DOF	1st	2nd	3rd	4th
1st	-4.17 (0.73)	-8.49 (1.16)	N/A	N/A
2nd	-6.11 (1.8)	-3.63 (1.65)	-1.59 (2.86)	N/A
3rd	N/A	14.4 (2.51)	9.83 (2.04)	7.29 (1.4)
4th	N/A	N/A	4.77 (3.29)	6.91 (1.24)

Fig. 8 Damage Pattern 6: Removing one plate at the third floor +DP5

Therefore, the resultant 7.29% change at DF_{34} is due to the superimposition of 5.6% stiffness reduction, and 12% mass reduction at the third floor ([(1-0.056)/ (1-0.12)-1] = 7.29%). Regarding the 4th row of the damage feature table, as the stiffness between the third and fourth floor was inferred as 5.6%, the change of 4.8% at DF_{43} can be explained as the superimposition of 5.6% stiffness reduction and 10% mass reduction at the fourth floor ([(1-0.056)/(1-0.10)-1] = 4.8%). Finally, it is can be concluded that there were approximately 12% mass reduction at the third and fourth floors and 5.6% reduction in stiffness between the two floors.

4. Conclusions

This study presents an improved time series analysis method for damage detection and its experimental verifications. The methodology starts with mathematical transformation of the equation of motion in order to fit the ARMAX models. Once ARMAX models were created for different output-only acceleration clusters, the relative difference of the models' coefficients between the baseline and damage cases are computed as the damage feature. The experimental data from a laboratory-scale structure was introduced to verify the methodology. The results show that the method is very effective in reflecting changes of mass and stiffness simultaneously. In addition, the *DF* values show the severity of damage and its location accurately. However, when multiple changes of stiffness and mass occur at the same time at close locations, decoupling the information about the mass and stiffness change may require a detailed analysis as discussed. In the current form, the method is applicable typically for shear type structures which is relatively easy to anticipate the number of DOF. However, general structures contain various DOFs depending on the professional judgement of engineers, and it would not be feasible to capture all information from all DOFs. Therefore, plans have been drawn to conduct a deeper study to minimize such limitations.

References

Agarwal, S. and Mitra, M. (2014), "Lamb wave based automatic damage detection using matching pursuit and machine learning", *Smart Mater. Struct*., **23**(8), https://doi.org/10.1088/0964-1726/23/8/085012.

Assi, R., Youance, S., Bonne, A. and Nollet, M.J. (2016), "Effect of non-structural components on the modal properties of buildings using ambient vibration testing", *Proceedings of the Annual Conference of the Canadian Society for Civil Engineering.*

Balageas, D., Fritzen, C.P. and Guemes, A. (2006), *Structural Health Monitoring.* Wiley Online Library.

Bao, C.X., Hao, H. and Li, Z.X. (2013), "Integrated ARMA model method for damage detection of subsea pipeline system", *Eng. Struct.*, **48**, 176-192. https://doi.org/10.1016/j.engstruct.2012.09.033.

Bas, S., Apaydin, N.M., Ilki, A. and Catbas, F.N. (2017), "Structural health monitoring system of the long-span bridges in Turkey", *Struct. Infrastruct. Eng*., 1-20. https://doi.org/10.1080/15732479.2017.1360365.

Bighamian, R. and Mirdamadi, H.R. (2013), "Input/output system identification of simultaneous mass/stiffness damage assessment using discrete-time pulse responses, differential evolution algorithm, and equivalent virtual damped SDOF", *Struct. Control Health Monit.*, **20,** 576-592. https://doi.org/10.1002/stc.516.

Box, G.E., Jenkins, G.M. and Reinsel, G.C. (2016), *Time Series Analysis: Forecasting and Control.* Prentice-Hall, Upper Saddle River, NJ.

Celik, O., Terrell, T., Necati, C.F. and Gül, M. (2018), "Sensor clustering technique for practical structural monitoring and maintenance", *Struct. Monit. Maint.*, **5**(2), 273-295. https://doi.org/10.12989/smm.2018.5.2.273.

Devin, A. and Fanning, P.J. (2012), "The evolving dynamic response of a four storey reinforced concrete structure during construction", *Shock Vib*., **19**(5), 1051-1059. https://doi.org/10.1155/2012/260926.

Fan, W. and Qiao, P. (2011), "Vibration-based damage identification methods: A review and comparative study", *Struct. Health Monit*., **1**(2), 83-111. https://doi.org/10.1088/0964-1726/1/2/002.

Figueiredo, E., Park, G.H., Farinholt, K.M., Farrar, C.R. and Lee, J.R. (2012), "Use of time-series predictive models for piezoelectric active-sensing in structural health monitoring applications", *J. Vib. Acoust*., **134** (4), 041014 -041014. https://doi.org/10.1115/1.4006410.

Gül, M. and Catbas, F.N. (2009), "Statistical pattern recognition for structural health monitoring using time series modeling: Theory and experimental verifications", *Mech. Syst. Signal Pr*., **23**, 2192-2204. https://doi.org/10.1016/j.ymssp.2009.02.013.

Gül, M. and Catbas, F.N. (2011), "Structural health monitoring and damage assessment using a novel time series analysis methodology with sensor clustering", *J. Sound Vib*., **330**(6), 1196-1210. https://doi.org/10.1016/j.jsv.2010.09.024.

Gül, M. and Catbas, F.N. (2008), "A new methodology for identification, localization and quantification of damage by using time series modeling", *Proceedings of the 28th International Modal Analysis Conference (IMAC XXVI)*, Florida.

He, K. and Zhu, W.D. (2011), "A vibration-based structural damage detection method and its applications to engineering structures", *Int. J. Smart Nano Mater*., **2**(3), 194-218. https://doi.org/10.1080/19475411.2011.594105.

Kuwabara, M., Yoshitomi, S. and Takewaki, I. (2013), "A new approach to system identification and damage detection of high-rise buildings", *Struct. Control Health Monit*., **20**, 703-727. https://doi.org/10.1002/stc.1486.

Levy, H. and Lessman, F. (1961), *Finite Difference Equations*, Courier Corporation.

Li, S. and Wu, Z. (2007), "Development of distributed long-gage fiber optic sensing system for structural health monitoring", *Struct. Health Monit*., **6**(2), 133-143. https://doi.org/10.1177/1475921706072078.

Loh, C.H., Chen, C.H. and Hsu, T.Y. (2011), "Application of advanced statistical methods for extracting long-term trends in static monitoring data from an arch dam", *Struct. Health Monit*., **10**(6), 587-601.

Lu, Y. and Gao, F. (2005), "A novel time-domain auto-regressive model for structural damage diagnosis", *J. Sound Vib*., **283**(3), 1031-1049.

Mehdi, S. (2010), "Vibration serviceability of a building floor structure. I: Dynamic testing and computer modeling", *J. Perform. Constr. Fac*., **24**(6), 497-507. https://doi.org/10.1061/(ASCE)CF.1943-5509.0000134.

Mei, Q. and Gül, M. (2015), "Novel sensor clustering - Based approach for simultaneous detection of stiffness and mass changes using output-only data", *J. Struct. Eng*., **141**(10), 04014237. https://doi.org/10.1061/(ASCE)ST.1943-541X.0001218.

Montgomery, D.C., Jennings, C.L. and Kulahci, M. (2008), *Introduction to Time Series Analysis and Forecasting.* Hoboken, New Jersey : Wiley-Interscience, 2008.

Nguyen, C.U., Huynh, T.C. and Kim, J.T. (2018), "Vibration-based damage detection in wind turbine towers using artificial neural networks", *Struct. Monit. Maint*., **5**(4), 507-519. https://doi.org/10.12989/smm.2018.5.4.507.

Omenzetter, P. and Brownjohn, J.M.W. (2006), "Application of time series analysis for bridge monitoring", *Smart Mater. Struct*., **15**(1), 129 -129. .

Peter Carden, E. and Brownjohn, J.M.W. (2008), "ARMA modelled time-series classification for structural health monitoring of civil infrastructure", *Mech. Syst. Signal Pr*., **22**(2), 295-314. https://doi.org///dx.doi.org/10.1016/j.ymssp.2007.07.003.

Takewaki, I. and Nakamura, M. (2000), "Stiffness-damping simultaneous identification using limited earthquake records", *Earthq. Eng. Struct. D*., **29**, 1219-1238.

Roy, K., Bhattacharya, B. and Ray-Chaudhuri, S. (2015), "ARX model-based damage sensitive features for structural damage localization using output-only measurements", *J. Sound Vib*., **349**, 99-122. https://doi.org/10.1016/j.jsv.2015.03.038.

Rytter, A. (1993), "Vibration Based Inspection of Civil Engineering Structures, 1993", Ph. D. dissertation.

Shahidi, S.G., Nigro, M.B., Pakzad, S.N. and Pan, Y. (2015), "Structural damage detection and localisation using multivariate regression models and two-sample control statistics", *Struct. Infrastruct. Eng.*, **11**(10), 1277-1293 -1277-1293. https://doi.org/10.1080/15732479.2014.949277.

Siebel, T., Friedmann, A., Koch, M. and Mayer, D. (2012), "Assessment of mode shape-based damage detection methods under real operational conditions", *Proceedings of the 6th European Workshop on Structural Health Monitoring*.

Soman, R., Kyriakides, M., Onoufriou, T. and Ostachowicz, W. (2017), "Numerical evaluation of multi-metric data fusion based structural health monitoring of long span bridge structures", *Struct. Infrastruct. Eng.*, 1-12. https://doi.org/10.1080/15732479.2017.1350984.

Sony, S., Laventure, S. and Sadhu, A. (2019), "A literature review of next-generation smart sensing technology in structural health monitoring", *Struct. Control Health Monit.*, **26**(3), https://doi.org/10.1002/stc.2321.

Takewaki, I. and Nakamura, M. (2005), "Stiffness-damping simultaneous identification under limited observation", *J. Eng. Mech. -ASCE*, **131**, 1027-1035. https://doi.org/10(1027).

Xi, P.S., Ye, X.W., Jin, T. and Chen, B. (2018), "Structural performance monitoring of an urban footbridge", *Struct. Monit.Maint.*, **5**(1), 129-150. https://doi.org/10.12989/smm.2018.5.1.129.

Zhang, D. and Johnson, E.A. (2013a), "Substructure identification for shear structures I: substructure identification method", *Struct. Control Health Monit.*, **20**, 804-820. https://doi.org/10.1002/stc.1497.

Zhang, D. and Johnson, E.A. (2013b), "Substructure identification for shear structures II: Controlled substructure identification", *Struct. Control Health Monit.*, **20,** 821-834. https://doi.org/10.1002/stc.1498.

JK